Draft version February 19, 2026
Typeset using LaTeX default style in AASTeX631

Periodic Wobble of the Post-Perihelion Jet Structure Around 3I/ATLAS

Toni Scarmato[1] and Abraham Loeb[2]

[1] *Toni Scarmato's Astronomical Observatory, San Costantino di Briatico, Calabria, 89817, Italy*
[2] *Astronomy Department, Harvard University, 60 Garden Street, Cambridge MA 02138, USA*

ABSTRACT

We analyse data on the post-perihleion morphology, including jet position angles (PAs) and coma-dominated photometry of the interstellar object 3I/ATLAS. From *Hubble Space Telescope* (HST) images processed with a Larson–Sekanina rotational-gradient filter, we measure the PAs of three main persistent jet-like features between November 30 and December 27, 2025 and fit a weighted Fourier model in a period scan. The dominant jet PA wobble yields $P_{\rm jet} = 7.20 \pm 0.05$ h. An independent G_r ($\approx R$) time-series photometry data set, using two different apertures from MPC station L92, analyzed with nightly offsets and 30-minute binning, gives $P_{\rm phot} = 7.136 \pm 0.001$ h (formal 1σ), with a semi-amplitude $A \simeq 0.311$ mag and scatter $\sigma_{\rm jit} \simeq 0.089$ mag. The close agreement beetwen the periods supports a characteristic post-perihelion period of ~ 7.1 h. We interpret this period as an attitude precession/nutation (non-principal-axis rotation) traced by jet orientation and coma flux redistribution. The jet structure precesses about the rotation axis with a characteristic angular excursion of order $\sim 20^\circ$, and the rotation axis is aligned with the sunward direction to within $\sim 20^\circ$.

Keywords: comets: general — interstellar: individual (3I/ATLAS) — methods: data analysis — techniques: photometric — techniques: image processing

1. INTRODUCTION

Jets are among the most direct probes of cometary nucleus activity. Time-variable jet position angles (PAs) and coma brightness modulations can constrain rotation, precession, and the distribution of active areas (e.g., Larson & Sekanina 1984; Jewitt 1997; Samarasinha et al. 2004; Farnham & Schleicher 2005). Coma-dominated photometry does not necessarily trace the spin of a bare nucleus: instead, it often reflects a time-dependent mapping from jet geometry and dust production into the chosen aperture. Non-principal-axis (NPA) rotation and precession can produce quasi-periodic PA "wobbles" and non-sinusoidal waveforms, particularly when the coma evolves into fan-like structures (e.g., Samarasinha & A'Hearn 1991; Belton et al. 2010).

For unevenly sampled time series, period searches commonly rely on the Lomb–Scargle formalism and its generalizations (Lomb 1976; Scargle 1982; Zechmeister & kürster 2009). When the observable is non-sinusoidal, truncated Fourier-series representations provide a compact model solvable by linear least squares at fixed trial period (e.g., Press et al. 2007).

In a previous paper (Scarmato & Loeb 2026) we derived: (i) a jet-PA period scan from the Hubble Space Telescope (HST) image morphology and (ii) an independent ground-based photometric period search to constrain the activity and period of 3I/ATLAS. That analysis identified a jet-PA wobble period $P_{\rm jet} = 7.20 \pm 0.05$ h from HST epochs spanning November 30–December 27, 2025 and a photometric period $P_{\rm phot} = 7.136 \pm 0.001$ h from 30-minute binned G_r-band photometry obtained on four nights. The periods are not identical at the formal level, but their similarity is consistent with non-Gaussian systematics, aliasing, and the different transfer functions between nucleus attitude, jet morphology, and coma-integrated flux. Our goal here is to interpret the inferred ~ 7.1 h period explicitly in terms of an attitude precession/nutation signature, and to connect it to multi-jet geometry and aperture-dependent photometric responses as the inner coma transitions between collimated and fan-like morphologies.

2. OBSERVATIONS AND DATA

2.1. *Morphology and jet PA measurements*

Within the coma, we find evidence for three jets, separated equally from each other, by $\approx 120^\circ$ in the sky, in addition to the anti-tail outflow which extends toward the Sun out to a much longer distance. PAs are measured east of north in the plane of the sky. Jet 2 is approximately anti-sunward and close to the projected spin-axis direction inferred from the global morphology. Figure 1 summarizes the geometry and the mean jet PAs with their measured oscillation half-amplitudes.

2.2. *Photometry and Astrometrica apertures*

Photometry was performed with Astrometrica using circular apertures. Astrometrica adopts an effective aperture radius (N+0.5) pixels due to the fractional weighting of pixels at the aperture boundary. For a plate scale of $1.38''$ px^{-1}, the effective radii are $r_{\rm eff} \approx 6.2''$ for $N = 4$ and $r_{\rm eff} \approx 42.2''$ for $N = 30$.

3. METHODS

3.1. *Harmonic representation of PA oscillations*

We describe the PA time series with a k-harmonic representation,

$$\mathrm{PA}(t) = \mathrm{PA}_0 + \sum_{k=1}^{k} A_k \sin\left(\frac{2\pi k}{P_{\rm prec}} t + \phi_k\right), \tag{1}$$

where $P_{\rm prec}$ is interpreted as an attitude precession period. We use $k = 1$ and $k = 2$.

3.2. *Photometric folding and stationary tests*

Coma photometry is folded at trial periods near $P_{\rm prec} \sim 7.1$ h. We assess variability by comparing four-night and five-night folds, allowing per-night offsets and an added jitter term to represent coma evolution and seeing-dependent systematics.

4. RESULTS

4.1. *Dominant jet structure: PA wobble period from HST morphology*

Using HST images processed through a Larson–Sekanina Rotational-Gradient Filter (with typical settings of $\delta r = 0.1$ and $\Delta\theta = 31^\circ$), we measured the PAs of the dominant jet-like structure across epochs spanning 2025 November 30th–December 27th. A weighted period scan with a truncated Fourier representation (up to $k = 2$ harmonics) yields a best-fitting wobble period

$$P_{\rm jet} = 7.20 \pm 0.05 \text{ h}, \tag{2}$$

where the uncertainty is dominated by sparse sampling and morphology-dependent systematics (we adopt $\sigma_{\rm PA} = 3^\circ$ per measurement). The associated PA excursion is of order $\sim 20^\circ$ and the inferred projected axis is aligned with the sunward direction to within $\sim 20^\circ$.

4.2. *Coma photometry: small-aperture solution ($r_{\rm eff} \approx 6.2''$)*

Ground-based time-series photometry (MPC station code L92; G_r band $\approx R$), was extracted using Astrometrica with an aperture of $N = 4$ pixels (effective radius $r_{\rm eff} \approx (N + 0.5) \times 1.38'' \approx 6.2''$) shows a coherent modulation over a four-night subset after allowing nightly offsets and 30-minute binning. A Fourier-series period scan returns

$$P_{\rm phot} = 7.136 \pm 0.001 \text{ h} \tag{3}$$

with a formal 1σ uncertainty, semi-amplitude $A \simeq 0.311$ mag, and additional scatter $\sigma_{\rm jit} \simeq 0.089$ mag. Because the measured flux is coma-dominated, we treat the formal uncertainty as a lower bound: systematic effects (seeing, aperture losses, morphology changes) can dominate over photon noise.

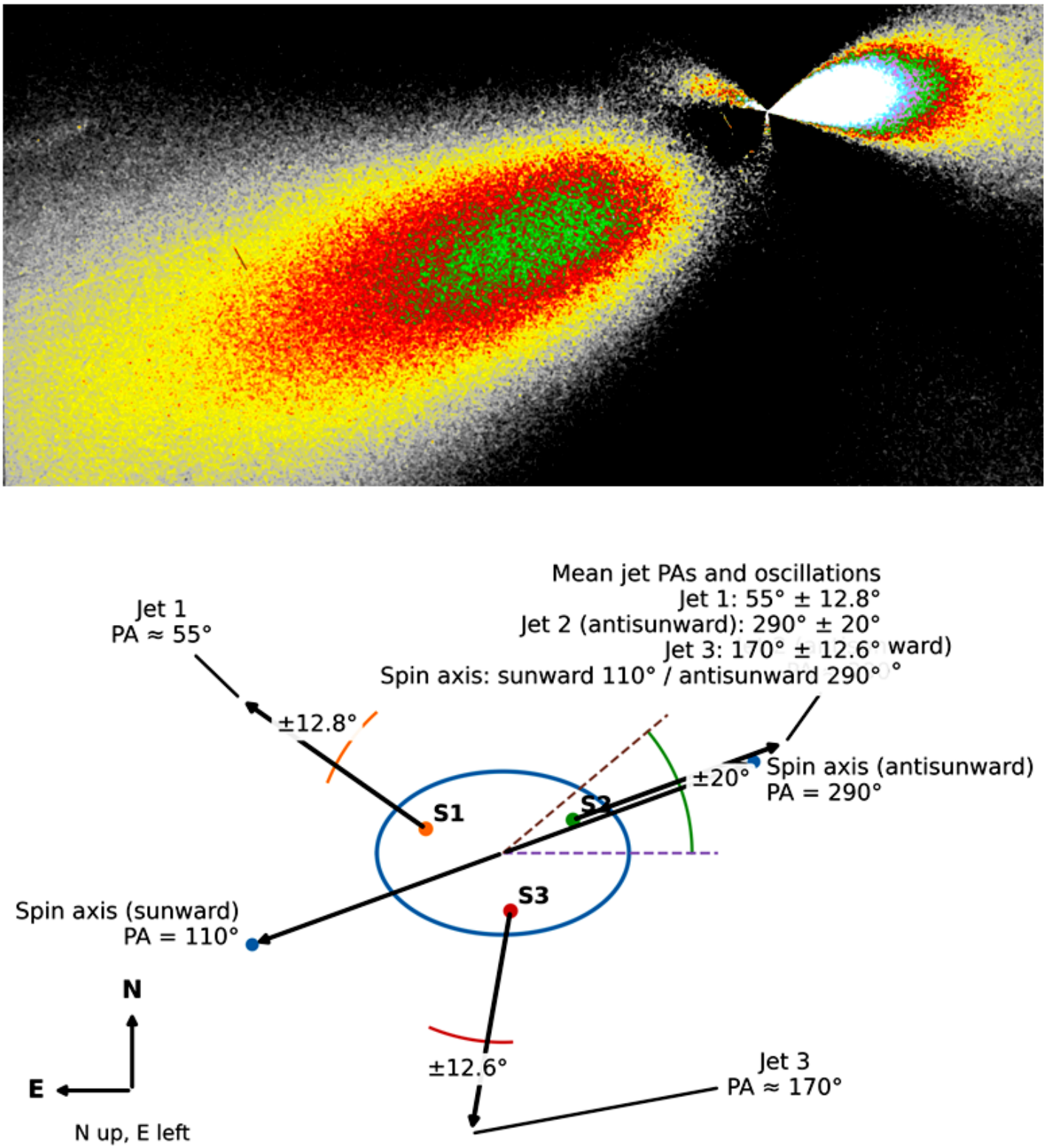

Figure 1. Schematic geometry (not to scale), with North up and East to the left. The projected spin axis is indicated in the sunward direction (PA= 110°) and anti-sunward direction (PA= 290°). Mean jet PAs and measured PA oscillation half-amplitudes are: Jet 1, $55^\circ \pm 12.8^\circ$; Jet 2 (anti-sunward), $290^\circ \pm 20^\circ$; Jet 3, $170^\circ \pm 12.6^\circ$. The scheme show the anti-sunward jet in PA=290° wobbling with period of 7.2 h, that is dominant in the photometric variation also.

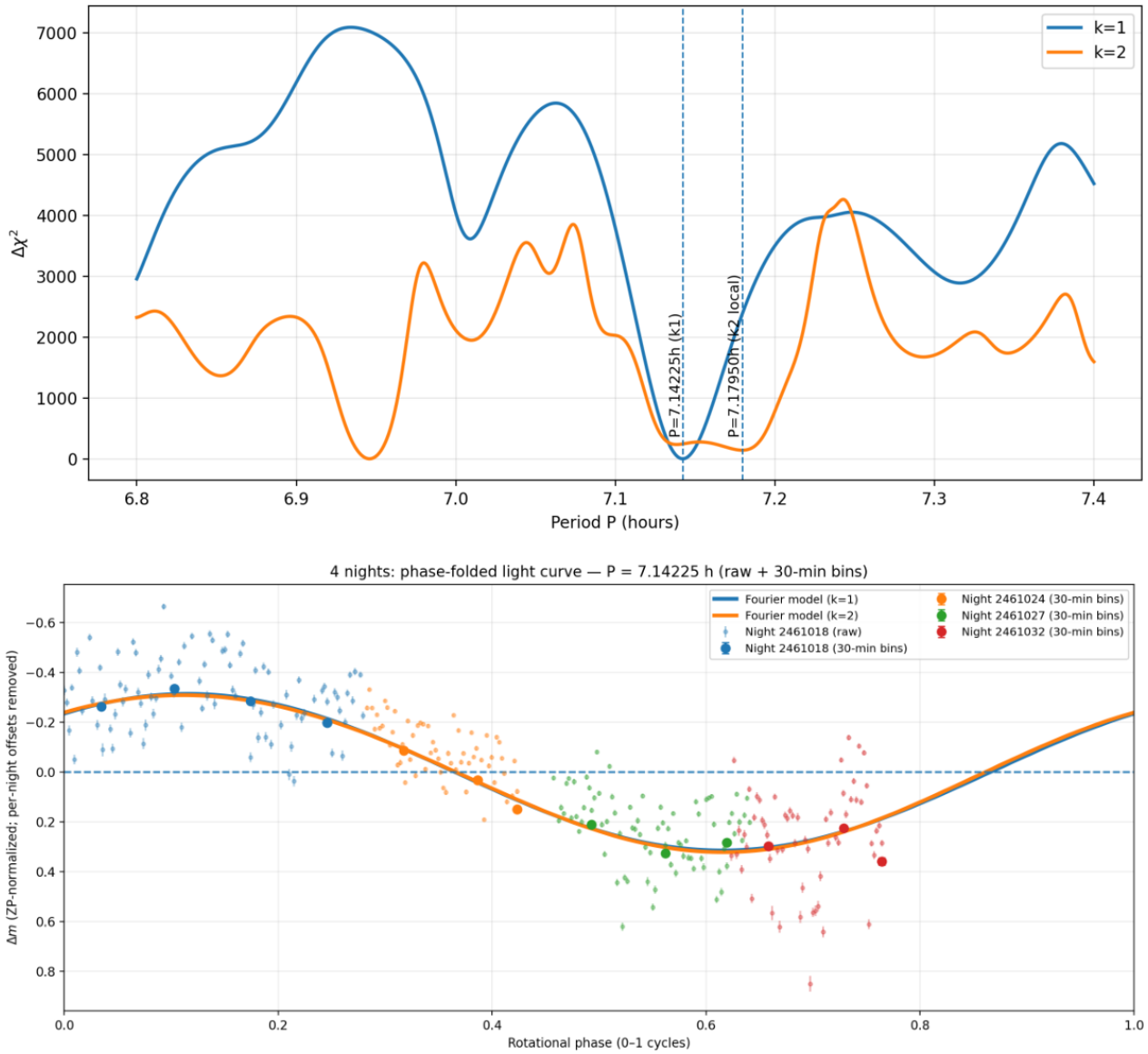

Figure 2. Large-aperture ($N = 30$, $r_{\rm eff} \approx 42.2''$) photometry: four-night subset. Top: $\Delta\chi^2$ period scan over 6.8–7.4 h for $k = 1$ and $k = 2$ Fourier models (per-night offsets allowed). Bottom: phase-folded light curve at $P = 7.142$ h after removing per-night offsets; the $k = 2$ model refines the waveform shape while preserving inter-night phase coherence.

4.3. *Coma photometry: large-aperture solution ($r_{\rm eff} \approx 42.2''$)*

We repeated the photometric analysis with a larger Astrometrica aperture of $N = 30$ pixels (effective radius $r_{\rm eff} \approx 42.2''$), designed to capture a broader coma region that is sensitive to fan-like jet opening.

In the physically motivated window 6.8–7.4 h, the best periods are:

- *four-night subset* ($N = 285$ points): $P_{\rm best}(k{=}1) = 7.142$ h and $P_{\rm local}(k{=}2) = 7.179$ h, with RMS ≈ 0.147 mag (Figure 2);
- *five-night full set* ($N = 398$ points): $P_{\rm best}(k{=}1) = 7.158$ h and $P_{\rm local}(k{=}2) = 7.175$ h, with RMS decreasing from ≈ 0.161 mag ($k{=}1$) to ≈ 0.156 mag ($k{=}2$) (Figure 3).

Including December 27, 2025 degrades phase stationarity relative to the four-night subset, consistent with the appearance of fan-shaped jets and a changing jet-to-photometry transfer function (Figure 4).

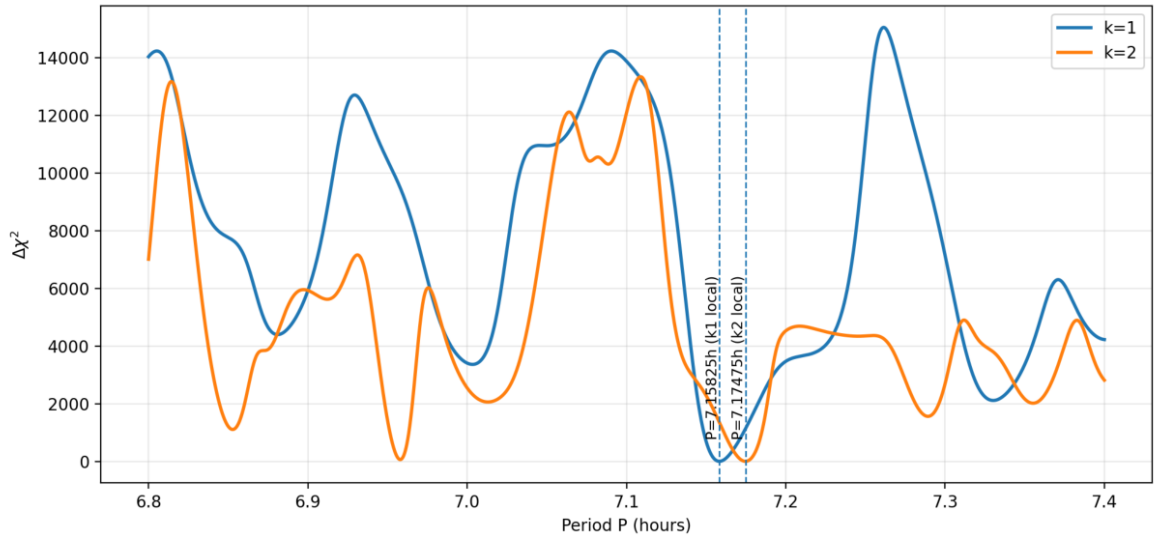

Folded using the 4-night reference period P = 7.14225 h (to highlight the degradation):

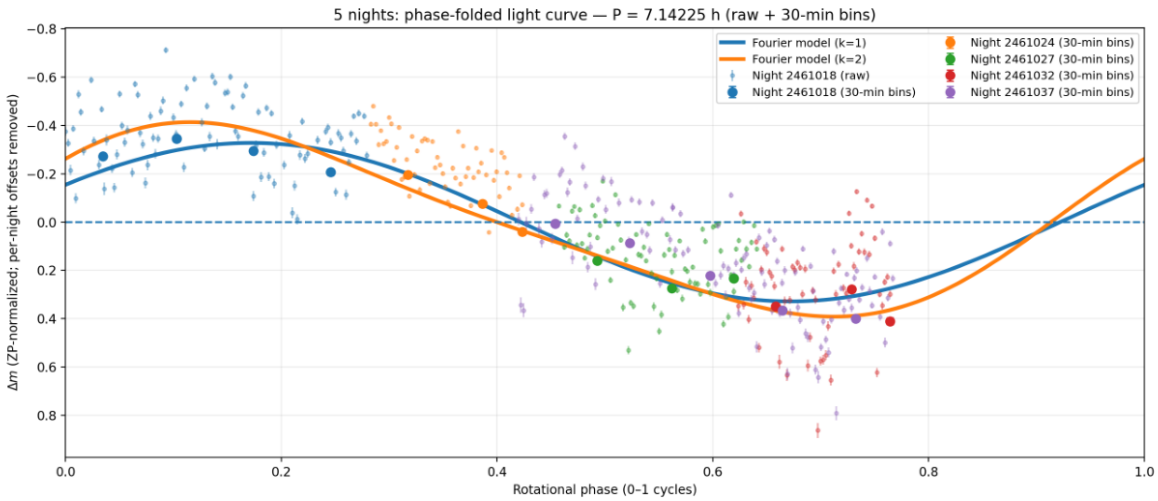

Folded using the best k=1 period from the 5-night scan (P = 7.15825 h):

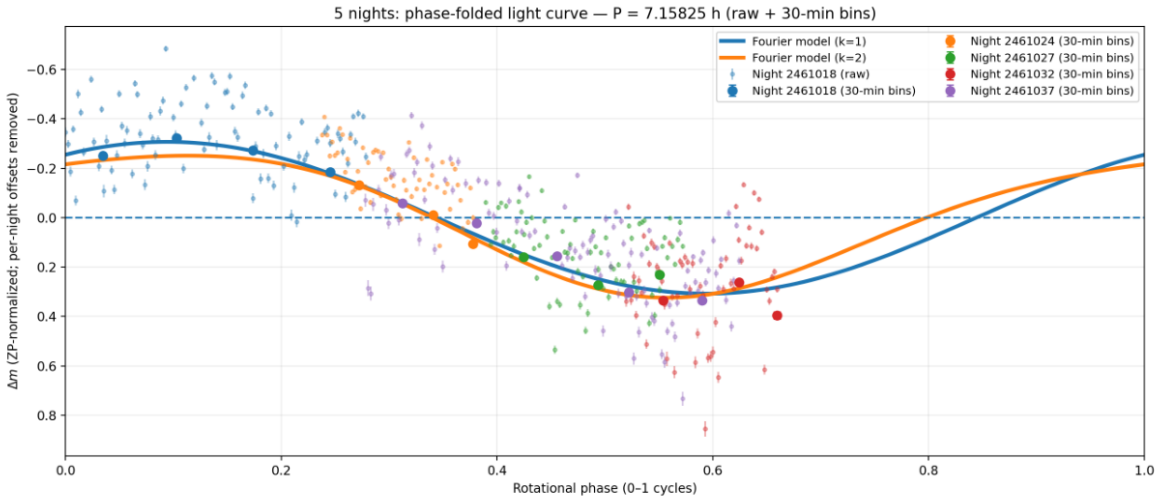

Figure 3. Same as Figure 2, but for the full five-night data set including December 27, 2025. Top: period scan within 6.8–7.4 h. Middle: fold at the four-night reference period $P = 7.142$ h highlighting degraded stationarity introduced by the fifth night. Bottom: fold at the best $k = 1$ period from the five-night scan, $P = 7.158$ h.

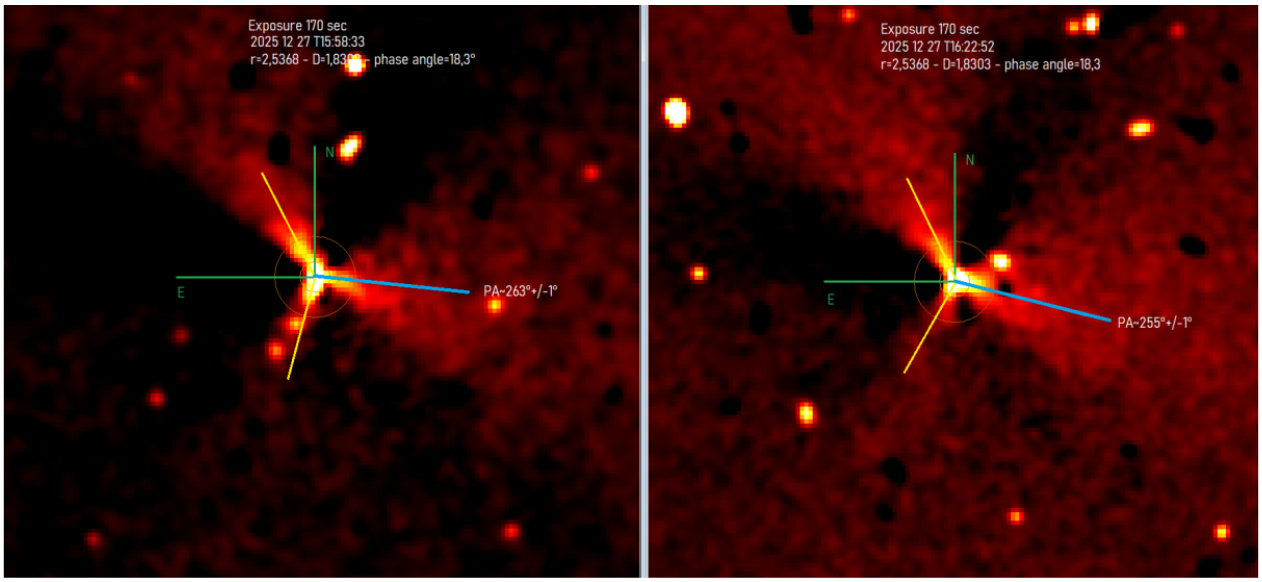

Figure 4. Inner-coma jets of 3I/ATLAS on 2025-12-27 UT. Two principal jet structures remain separated by $\sim 120°$, but the emission broadens into a fan. Such morphological changes modulate the coma brightness within a fixed aperture and can alter the amplitude/shape (and sometimes the apparent phase) of the photometric signal.

4.4. *Minor jets: additional PA periodicity from Jet 2 and Jet 3*

Independent PA time series for the secondary and tertiary jet structure yield shorter best-fit periods from weighted sinusoid+trend fits of the form $\mathrm{PA}(t) = c_0 + c_1 t + a\sin(2\pi t/P) + b\cos(2\pi t/P)$, where the linear term captures slow baseline drifts across nights.

Jet 2.—For Jet 2, the best period is $P_2 = 2.911$ h with amplitude $A_2 = 12.8°$ and a slow drift $c_1 = 0.009$ deg h^{-1} (≈ 0.22 deg day^{-1}). Assuming the reported $\pm 3°$ values represent 3σ (so $\sigma = 1°$), the reduced χ^2 at the best period is $\chi^2_\nu \simeq 3.0$, indicating additional systematics. Strong alias minima occur at $P \approx 4.432$ h, 3.739 h, 3.199 h, and 2.384 h (see Figure 5).

Jet 3.—For Jet 3, the best period is $P_3 = 4.299$ h with amplitude $A_3 = 12.6°$ and reduced chi-square $\chi^2_\nu \simeq 1.50$. The next-best local minima (aliases) occur at $P = 4.111$ h, 8.983 h, 5.983 h, 2.827 h and 3.602 h (see Figure 6).

Given sparse sampling and evolving coma morphology, we treat P_2 and P_3 as likely aliases/harmonics or feature-specific responses rather than independent nucleus spin periods. In a precession framework, such apparent shorter periods can arise from non-sinusoidal projection, multi-lobed emission, or morphology-dependent centroiding of the brightest streamline within a fan.

4.5. *Summary of periods*

Table 1 summarizes the periods derived from morphology and photometry. Despite differences at the formal level, the dominant jet PA wobble and the coma photometry cluster near a characteristic post-perihelion period of ~ 7.1 h when interpreted as an attitude/precession timescale. The shorter Jet 2 and Jet 3 periods are included as secondary/feature-tracing signals.

5. DISCUSSION

5.1. *Precession (NPA) interpretation of the 7.1 h period*

We interpret the ~ 7.1 h periodicity as an attitude precession/nutation period in a non-principal-axis (NPA) rotation state, rather than as a nucleus-shaped rotational light curve. In an NPA state, projected body axes (and any fixed active regions on the surface) can undergo a quasi-periodic wobble as the nucleus precesses about the angular-momentum

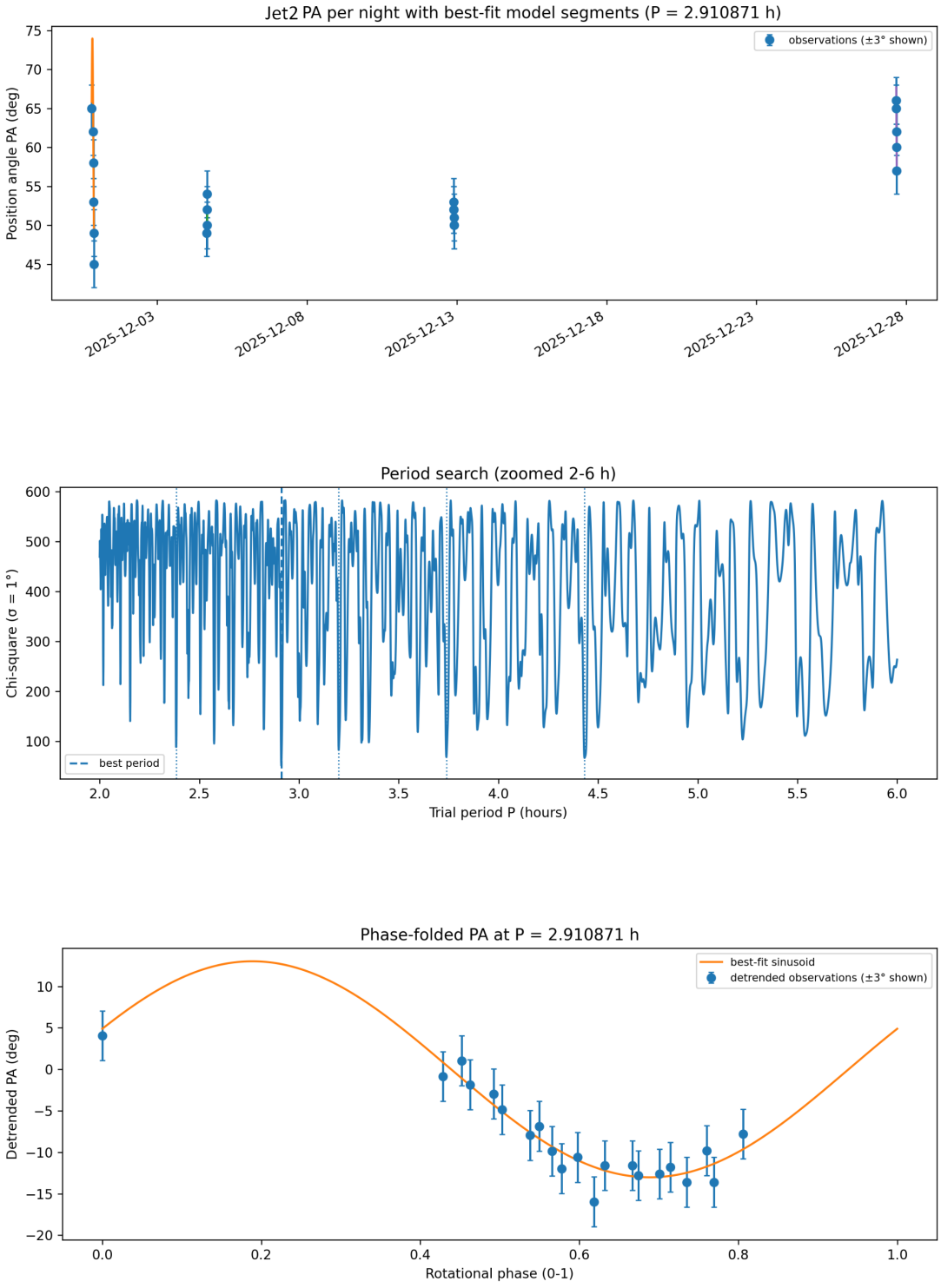

Figure 5. Jet 2 diagnostic plots from the PA time series analysis: (top) PA versus time by observing segment with the best-fit model drawn within each night; (middle) period scan (2–6 h zoom); (bottom) detrended phase fold at $P_2 = 2.9$ h. Error bars correspond to the reported ±3° values.

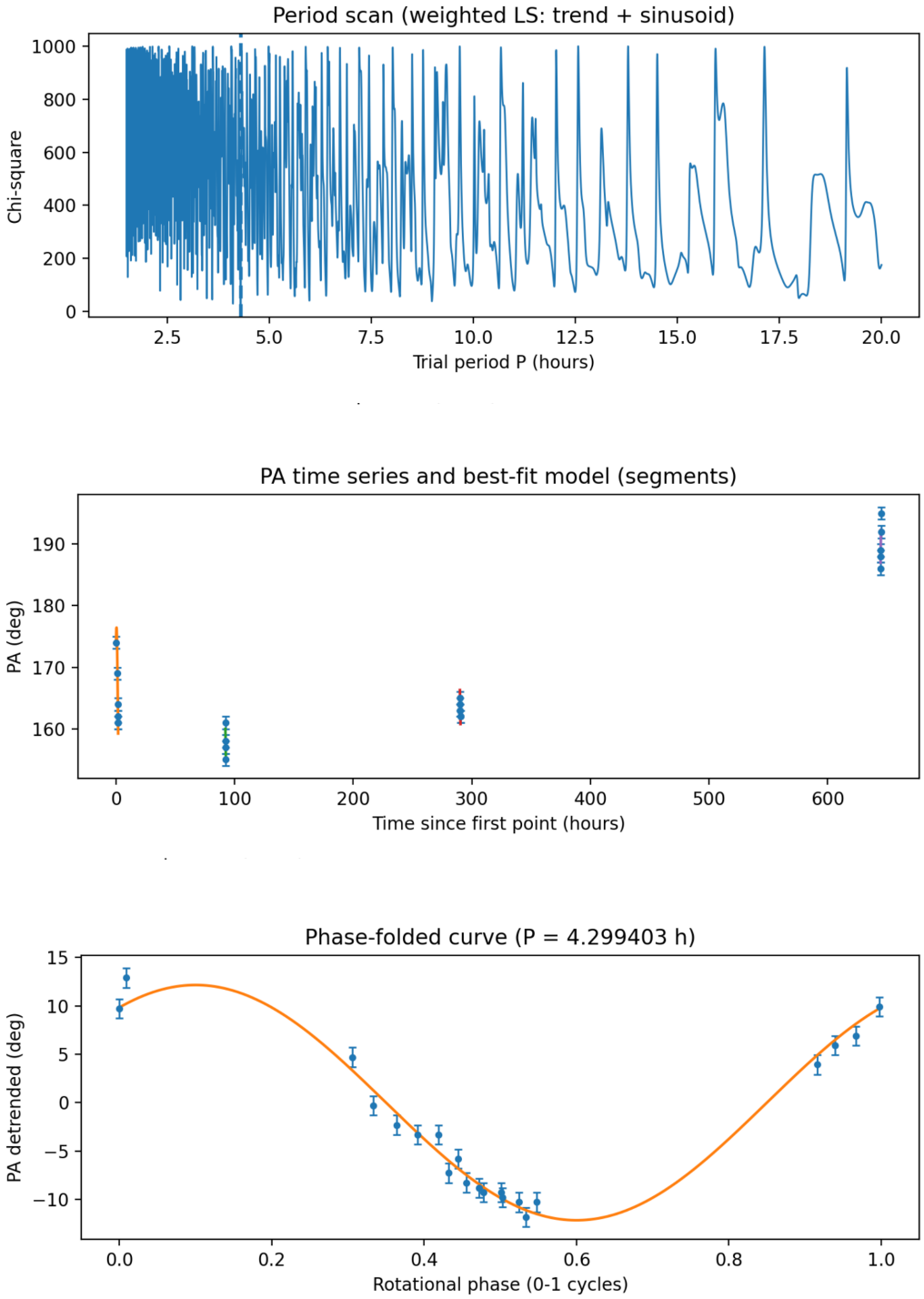

Figure 6. Jet 3 diagnostic plots from the PA time series analysis: (top) period scan; (middle) PA versus time by observing segment with best-fit model segments; (bottom) detrended phase fold at $P_3 = 4.3$ h.

Table 1. Summary of periodic signals used in this work.

Tracer	Data / method	Best period (h)	Notes
Dominant jet PA wobble	HST morphology; Fourier ($k \leq 2$) scan	7.20 ± 0.05	$\sigma_{\rm PA} = 3^\circ$;
Coma photometry (small)	L92; Astrometrica $N = 4$ ($r_{\rm eff} \approx 6.2''$)	7.136 ± 0.001	$A \simeq 0.311$ mag; $\sigma_{\rm jit} \simeq 0.089$ mag
Coma photometry (large, 4 nights)	L92; Astrometrica $N = 30$ ($r_{\rm eff} \approx 42.2''$)	7.142	RMS ≈ 0.147 mag
Coma photometry (large, 5 nights)	L92; Astrometrica $N = 30$ ($r_{\rm eff} \approx 42.2''$)	7.158	RMS ≈ 0.161 mag ($k = 1$)
Jet 2 PA	PA(t) sinusoid+trend fit	2.911	$A_2 \simeq 13^\circ$;
Jet 3 PA	PA(t) sinusoid+trend fit	4.299	$A_3 \simeq 12^\circ$;

vector (e.g., Samarasinha & A'Hearn 1991; Belton et al. 2010). This naturally explains: (i) PA oscillations about mean directions with feature-dependent amplitudes and phases, (ii) non-sinusoidal waveforms that result from $k = 2$ terms, and (iii) sensitivity to evolving collimation (fan opening) that can distort the observed waveform without requiring a change in the underlying period.

5.2. *Why coma photometry follows the precession period*

Because the measured flux is coma-dominated, the photometric modulation is best interpreted as an activity response: precession-driven variation in the projected jet directions and collimation, changes the fraction of jet and near-nucleus dust flux within a fixed observing aperture. A decisive test is phase locking: if the modulation is jet-driven, extrema in magnitude should correlate with the precession phase inferred from PA(t), potentially with a lag representing dust transport and seeing/aperture smoothing.

5.3. *Aperture dependence as a diagnostic*

The comparison between $r_{\rm eff} \approx 6.2''$ and $42.2''$ provides a direct test of a jet-driven period. If the modulation were a bare-nucleus rotational light curve, the inferred period and waveform would be insensitive to aperture size. Instead, the large-aperture solution exhibits degraded stationarity when the coma transitions to a fan-like morphology (December 27, 2025; see Figure 4) and shows modest shifts in preferred periods within the 6.8–7.4 h window (Table 1). This is expected if the measured flux is a convolution of intrinsic activity with dust transport, seeing, and aperture-dependent redistribution.

5.4. *Can multiple jets "stabilize" the nucleus?*

Multiple active sources can partially cancel net outgassing torques, helping to keep the angular-momentum direction relatively stable in inertial space. However, torque cancellation does not imply an absence of rotation; rather, it can allow the nucleus to maintain a long-lived non-principal-axis state with a slowly evolving angular-momentum vector. In this context, Jet 2—approximately anti-sunward and close to the projected rotation axis—anchors the large-scale morphology, while Jets 1 and 3 trace the precession cone through their PA oscillations. The observed ~ 7.1 h period is then interpreted as an attitude precession/nutation timescale that modulates both the projected jet directions and the inner-coma flux captured by fixed apertures.

6. CONCLUSIONS

We analyze data showing a coherent post-perihelion activity period in 3I/ATLAS, traced independently by inner-coma jets morphology and coma-dominated photometry. Our main findings are:

1. A dominant jet-like feature in HST images shows a repeatable PA wobble with $P_{\rm jet} = 7.20 \pm 0.05$ h from a weighted Fourier ($k \leq 2$) period scan, with an angular excursion of order $\sim 20^\circ$.

2. Small-aperture coma photometry ($N = 4$, $r_{\rm eff} \approx 6.2''$) yields $P_{\rm phot} = 7.136 \pm 0.001$ h (formal), with semi-amplitude $A \simeq 0.311$ mag and additional jitter $\sigma_{\rm jit} \simeq 0.089$ mag.

3. Large-aperture photometry ($N = 30$, $r_{\rm eff} \approx 42.2''$) gives best periods in the 7.14–7.16 h range for $k = 1$ fits, while the inclusion of December 27, 2025 (fan-like jets) degrades phase stationarity and slightly shifts preferred periods.

4. We interpret the ~ 7.1 h period as an attitude precession/nutation (NPA) signature traced by jet orientation and coma flux redistribution, rather than as a nucleus-shaped rotational light curve.

AKNOWLEDGEMENT AL was supported in part by the Galileo Project at Harvard University

REFERENCES

Belton, M. J. S., et al. 2010, Icarus, 210, 881

Farnham, T. L., & Schleicher, D. G. 2005, Icarus, 173, 533

Jewitt, D. 1997, Earth, Moon, and Planets, 79, 35

Larson, S. M., & Sekanina, Z. 1984, Astronomical Journal, 89, 571

Lomb, N. R. 1976, Astrophysics and Space Science, 39, 447

Press, W. H., Teukolsky, S. A., Vetterling, W. T., & Flannery, B. P. 2007, Numerical Recipes: The Art of Scientific Computing, 3rd edn. (Cambridge University Press)

Samarasinha, N. H., & A'Hearn, M. F. 1991, Icarus, 93, 194

Samarasinha, N. H., Belton, M. J. S., Mueller, B. E. A., et al. 2004, in Comets II, ed. M. C. Festou, H. U. keller, & H. A. Weaver (Tucson: University of Arizona Press), 281–299

Scarmato, T. Loeb, A., Rotation period of 3i/atlas after perihelion from jet position angle wobble and photometric variability. arXiv preprint arXiv:2601.10860, 2026.

Scargle, J. D. 1982, ApJ, 263, 835

Zechmeister, M., & kürster, M. 2009, A&A, 496, 577